Published in "Chemical Physics Letters 620: 29–34, 2015"
which should be cited to refer to this work.

Photon cascade emission in Pr^{3+} doped fluorides with CaF_2 structure: Application of a model for its prediction

Benjamin Herden[a], Amador García-Fuente[a], Harry Ramanantoanina[a], Thomas Jüstel[b], Claude Daul[a], Werner Urland[a,*]

[a] Department of Chemistry, University of Fribourg, Chemin du Musée 9, 1700 Fribourg, Switzerland
[b] Department of Chemical Engineering, Münster University of Applied Sciences, Stegerwaldstrasse 39, 48565 Steinfurt, Germany

In this work, we predict and measure the optical behaviour of Pr^{3+} in different binary and ternary fluorides. We use a validated model based on Ligand Field Theory and Density Functional Theory to calculate the multiplet energy levels arising from the ground $[Xe]4f^2$ and excited $[Xe]4f^15d^1$ electron configurations of Pr^{3+} in its chemical environment. Moreover, the luminescence spectra of the considered materials were recorded. In overall the theoretical determination corroborates to the experimental findings. The phenomenon of the photon cascade emission is particularly stressed, being important for the design of modern phosphors with quantum efficiencies larger than 100%.

1. Introduction

Divalent and trivalent lanthanide ions are widely applied in phosphors, laser gain media and scintillator crystals or ceramics. Especially trivalent praseodymium (Pr^{3+}) shows a large variety of different applications as activator ion, viz. UV phosphors [1], laser materials [2], up- [3] and down-conversion [4,5] phosphors. The down-conversion phosphors also called quantum cutter systems or photon cascade emission materials (PCE), exhibit a two or more photon luminescence process, where at least two low energy photons are emitted per one high energy photon absorbed [6,7]. Therefore, quantum efficiencies larger than 100% are achievable. PCE materials can be useful in plasma display panels or Hg-free discharge lamps, in which the phosphors are excited by vacuum UV radiation from the Xe excimer discharge [8].

The observation of PCE in Pr^{3+} phosphors was simultaneously described by Sommerdijk et al. [4] and by Piper et al. [5] in 1974 for YF_3. There Piper et al. reported quantum efficiencies of about 140%, which have also been found for β-$NaLaF_4$ [9]. Aside the usual fluoride hosts, Pr^{3+} doped oxidic hosts, viz. $SrAl_{12}O_{19}$ [10], $LaMgB_5O_{10}$ [11], and LaB_3O_6 [12] were demonstrated to show PCE, whose phenomenon can only be observed if the lowest energy level of the excited $[Xe]4f^15d^1$ electron configuration of Pr^{3+} is located above the $^1S_0$ energy level of the ground $[Xe]4f^2$ electron configurations [5]. It is of crucial importance to delimitate the multiplet energy levels arising from the ground $[Xe]4f^2$ and the excited $[Xe]4f^15d^1$ electron configurations of Pr^{3+} in its chemical environment. It turns out that an overlap between both multiplet energy levels is controlled by a balance between two interactions such as the nephelauxetic effect and the ligand field splitting [13].

Since fluoride ligands exhibiting a small nephelauxetic effect [13], the position of the lowest energy level of the $[Xe]4f^15d^1$ configuration depends mainly on the ligand field splitting of the 5d orbitals. This ligand field splitting is mainly dependent on the coordination sphere of the Pr^{3+} ion.

We consider herein four different host matrices, (CaF_2, SrF_2, BaF_2, and α-$NaYF_4$) all crystallizing in the cubic CaF_2 structure type (space group $Fm-3m$). The Pr^{3+} is doped in the unique eightfold coordinated cation site having O_h symmetry [14]. The cubic α-phase of $NaYF_4$ is the high-temperature polymorph, unlike the low temperature one which possesses the hexagonal (space group $P-6$) β-phase [15]. In α-$NaYF_4$ the cation site is randomly occupied by ½ Na^+ and ½ Y^{3+} [16].

The luminescence of these Pr^{3+} activated fluorides has been experimentally described by several working groups [17–19]. The alkaline earth fluorides (CaF_2:Pr^{3+}, SrF_2:Pr^{3+}, and BaF_2:Pr^{3+}) show in all the cases broad band emission due to the fact that the lowest energy level of the $[Xe]4f^15d^1$ configuration is located below the $^1S_0$ energy level [17]. Thus the ligand field splitting of the 5d orbitals is expected to be large. On the other hand, the α-$NaYF_4$:Pr^{3+} shows line emission proper for PCE materials [18,19]. Here the ligand field interaction of the 5d orbitals is certainly weaker. These findings

* Corresponding author.
E-mail address: wurland@arcor.de (W. Urland).

cannot be solely explained by the different sizes of the replaced cations, Ca^{2+}: 126 pm, Sr^{2+}: 140 pm, Ba^{2+}: 156 pm and Y^{3+}: 116 pm in contrast to Pr^{3+}: 126.6 pm (all given for coordination number (CN) 8 [20]), since the chemical environment and the symmetry is in all cases identical. Rodnyi et al. [21] reported about the energy shift of the lowest level of the $[Xe]4f^15d^1$ configuration as function of the Pr^{3+} concentration in BaF_2 crystals. For higher concentrations (3.0%) PCE was observed due to the formation of Pr^{3+}-based clusters.

Here we apply our validated model [13] to explain and predict the above mentioned PCE phenomenon. This model is also essential for tailoring phosphors to generate warm-white light [22]. The structure of the Pr^{3+} doped systems is optimized using periodical calculations based on Density Functional Theory (DFT) by means of the VASP code [23,24]. The PBE functional is used to parameterize the exchange-correlation potential [25]. The structure of the doped system is obtained taking into account a super-cell model composed by one Pr^{3+} ion in 32 unit-cells corresponding to a dopant concentration of 3%. It is important to mention that the Pr^{3+} ions are handled as isolated ions. A selective cut of this optimized structure is performed taking into account the Pr^{3+} centre and its surrounding ligands, subjected to a molecular calculation using the Amsterdam Density Functional (ADF 2013.01) program package [26,27]. We use the computational model named LFDFT [13,28,29], whose output enables the computations of the Slater–Condon parameters, spin–orbit coupling constants and ligand field potential. Preparation and optical characterization of CaF_2:Pr^{3+},Na^+; SrF_2:Pr^{3+},Na^+; BaF_2:Pr^{3+},Na^+; and α-$NaYF_4$:Pr^{3+} are performed (see Section 4). The doping level was is all cases adjusted to 1.0% to avoid clustering of Pr^{3+} in the powder samples. The prepared phosphors were of single phase and luminescence spectra were recorded from the VUV to the near infrared region.

2. Results and discussion

The calculations for the Pr^{3+} doped alkaline earth fluorides and α-$NaYF_4$ yield the parameters listed in Table 1. In the table two columns are devoted to the α-$NaYF_4$ system relating the two special extreme situations which are illustrated by taking the second coordination sphere containing exclusively Na^+ (hereafter O_h(Na)) or Y^{3+} (hereafter O_h(Y)) ions. In both situations, O_h symmetry of the coordination of the Pr^{3+} is achieved.

Table 1
Electrostatic and ligand field parameters for all Pr^{3+} doped hosts with O_h site symmetry (in cm^{-1}).

Host	CaF_2	SrF_2	BaF_2	α-$NaYF_4$	α-$NaYF_4$
Symmetry	O_h	O_h	O_h	O_h(Na)	O_h(Y)
F_2(ff)[a]	322.8	322.9	322.9	322.9	322.8
F_4(ff)[a]	41.7	41.7	41.7	41.7	41.7
F_6(ff)[a]	4.4	4.4	4.4	4.4	4.4
G_1(fd)[a]	358.9	356.9	351.2	350.2	365.3
F_2(fd)[a]	226.7	225.3	222.7	221.4	229.4
G_3(fd)[a]	30.7	30.5	30.1	29.9	31.2
F_4(fd)[a]	17.4	17.3	17.1	17.0	17.6
G_5(fd)[a]	4.8	4.7	4.7	4.7	4.9
ζ_{4f}[b]	710	710	710	710	710
ζ_{5d}[b]	945	945	945	945	945
e_σ(f)[c]	599	538	491	450	673
e_π(f)[c]	257	232	213	164	279
e_σ(d)[c]	14 114	13 009	12 154	11 652	16 210
e_π(d)[c]	4705	4336	4051	3886	5404
Δ_{AOM}(fd)[d]	15 183	17 918	20 030	21 162	9851

[a] F_k(ff), F_k(fd) and G_k(fd) refer to the interelectronic effect known as Slater–Condon parameters widely described in textbooks [30,31].
[b] Spin–orbit coupling constants for the 4f and 5d orbitals were obtained using the relativistic ZORA approach [13].
[c] The ligand field interaction is better represented with respect to the Angular Overlap Model (AOM) parameters [32]. In the present case four AOM parameters are available due to the problem of two-open-shell 4f and 5d electrons.
[d] We refer to [32] and define Δ_{AOM}(fd) accordingly.

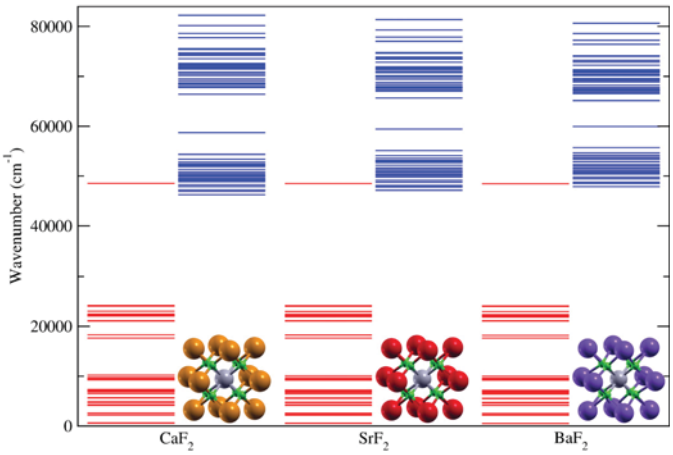

Figure 1. Calculated multiplet energy levels of Pr^{3+} doped CaF_2, SrF_2, and BaF_2 corresponding to the $[Xe]4f^2$ (red) and the $[Xe]4f^15d^1$ configurations (blue). The structures represent the central Pr^{3+} ion (grey) surrounded by eight F^- (green) and the second coordination sphere containing the corresponding alkaline earth cations. (For interpretation of the references to colour in this figure legend, the reader is referred to the web version of this article.)

The theoretical results are graphically represented in Figure 1, where the multiplet energy levels originating from the $[Xe]4f^2$ and the $[Xe]4f^15d^1$ configurations are given in red and blue, respectively. An overlap between both multiplet energy levels is noticed. Thus PCE is not observed as it is confirmed by our related experimental work (see Figure 2) which is also in line with earlier observations by Lawson et al. [17].

Due to the weak ligand field interaction of the 4f orbitals of Pr^{3+} (see parameters in Table 1), in Figure 1 the multiplet energy levels arising from the $[Xe]4f^2$ configurations seem to be identical in any systems. On the other hand, the influence of the chemical surrounding on the 5d orbitals is stronger which results in a different splitting of the $[Xe]4f^15d^1$ configurations. In the present situation the 5d orbitals of Pr^{3+} split over e_g and t_{2g} irreducible representations of the O_h point group. Therefore, the multiplet energy levels from the $[Xe]4f^15d^1$ configurations are split in two different bands fully recognized in Figure 1 but also in the experimental characterization below (see Figure 2).

The ionic radii of Ca^{2+} (126 pm) and Pr^{3+} (126.6 pm) for CN 8 are almost identical, whereas the ionic radii of Sr^{2+} (140 pm) and Ba^{2+} (156 pm) are much larger. This means, that the size of the cation which is replaced by Pr^{3+} is increasing (see Table 2) in the series of CaF_2, SrF_2 and BaF_2 leading to a decrease of the splitting for the 5d orbitals of Pr^{3+}. The total splitting of the calculated multiplet energy levels between e_g and t_{2g} is specified with 20 910 cm^{-1} for CaF_2:Pr^{3+}, 19 272 cm^{-1} for SrF_2:Pr^{3+}, and 18 006 cm^{-1} for BaF_2:Pr^{3+}.

The luminescence spectra of the Pr^{3+} doped alkaline earth fluorides are measured (see Section 4) and given in Figure 2. Since we focus on the lowest energy level of the $[Xe]4f^15d^1$ configuration, excitation spectra were monitored in the VUV part of the spectral range. The excitation spectra indicate that there are two separated bands which can be compared to the e_g and t_{2g} levels known for O_h symmetry. The splitting between these two bands is decreasing from about 18 230 cm^{-1} for CaF_2:Pr^{3+},Na^+(1.0%) and 14 580 cm^{-1} for SrF_2:Pr^{3+},Na^+(1.0%) to 13 260 cm^{-1} for BaF_2:Pr^{3+},Na^+(1.0%). The values were derived taking the energy difference between the two maxima of the excitation bands, whereat it is important to announce that the measurements were done at room temperature (298 K). Our theoretical results overestimate them by about 20%, although the case of CaF_2:Pr^{3+} are perfectly in line with the

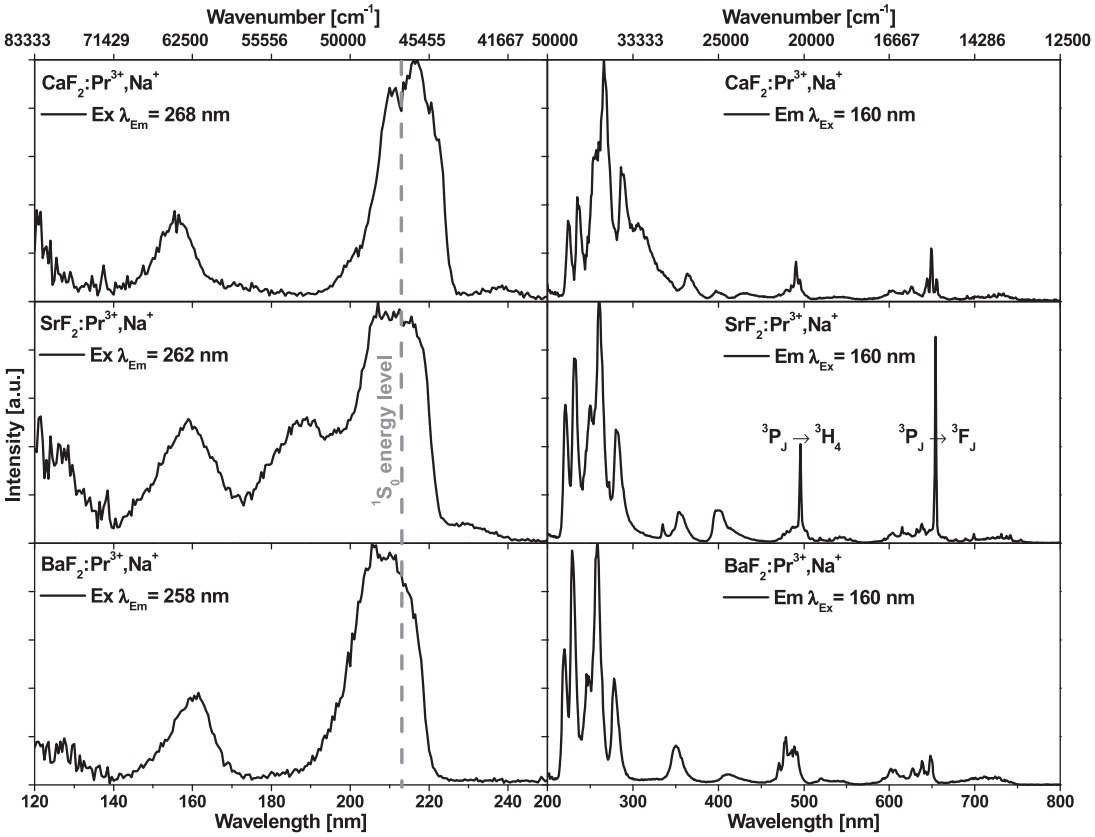

Figure 2. Room temperature luminescence spectra of CaF_2:Pr^{3+},Na^+(1.0%), SrF_2:Pr^{3+},Na^+(1.0%) and BaF_2:Pr^{3+},Na^+(1.0%). VUV excitation spectra are plotted on the left and emission spectra on the right. The dashed grey line represents the energy position of the $^1S_0$ energy level.

observation of Oskam et al. [35]. They reported a ligand field splitting of the 5d orbitals of about 21 000 cm^{-1} derived from experimental work (measured at 6 K). The discrepancy originates from the temperature dependence of the t_{2g} levels, meanwhile the e_g levels remain at the same energy. This was already observed by Loh [36] in former investigations of the UV absorption of Pr^{3+} doped alkaline earth fluorides. Since the e_g levels remain at the same energy, changes in the emission spectra cannot be observed. The highest energy level $^1S_0$ of the ground [Xe]$4f^2$ configuration is expected to be located close to 47 000 cm^{-1} as it is determined theoretically (see Figure 1) and which was already described in literature [4,35]. Therefore, the lowest energy level of the [Xe]$4f^1 5d^1$ configuration is in all cases overlapping with the highest energy level $^1S_0$. PCE for these phosphors is not observed whereby the emission spectra in Figure 2 mainly show broad band emission from the lowest energy level of the [Xe]$4f^1 5d^1$ configuration in the UV part of the spectral range. In case of SrF_2:Pr^{3+},Na^+ an intermediate band between the e_g and the t_{2g} ones appears which is due to a small amount of residual PrF_3 [37]. However, this leads to higher intensities of intraconfigurational [Xe]$4f^2$–[Xe]$4f^2$ transitions which can only be observed in the case of SrF_2:Pr^{3+},Na^+.

In comparison to the binary alkaline earth fluorides the ternary α-$NaYF_4$ is investigated. The α-polymorph exhibits the cubic CaF_2 structure type with Na^+ and Y^{3+} randomly distributed on the cation sites. Here, the average bond length is comparable to the one of CaF_2 (see Table 2).

The results of the calculations are given in Figure 3, following the same representations as in Figure 1. The two above mentioned extreme situations of the O_h symmetry are calculated separately. An overlap between both multiplet energy levels is noticed again. Thus PCE is not expected in both situations which is in contradiction to our experimental results (see Figure 4) and also to the experimental work published by Sommerdijk et al. [18].

The multiplet energy levels arising from the [Xe]$4f^2$ configurations in Figure 3 seem to be again nearly identical for the two different O_h situations. The influence of the chemical surrounding on the 5d orbitals is much stronger which results in a different splitting for the [Xe]$4f^1 5d^1$ configurations. Na^+ has a larger ionic radius than Y^{3+}, leading to smaller splitting of the 5d orbitals of Pr^{3+}. Therefore, the lowest energy level of the [Xe]$4f^1 5d^1$ configuration is located at higher energy but still below the $^1S_0$ energy level. The total splitting of the calculated multiplet energy levels between e_g and t_{2g} is specified with 17 255 cm^{-1} for O_h(Na) and 24 015 cm^{-1} for the O_h(Y) symmetry.

The luminescence spectra of α-$NaYF_4$:Pr^{3+}(1.0%) are given in Figure 4. The excitation spectrum shows one broad band ranging from 48 000 to 72 000 cm^{-1} with two next neighboured maxima. The highest energy level $^1S_0$ of the ground [Xe]$4f^2$ configuration is

Table 2
Cation–anion bond length in different hosts (in pm). Literature values give the bond length of the undoped hosts whereas the calculated ones display the values of the theoretical Pr–F bond. In case of α-$NaYF_4$ the distance from the literature shows the average value.

Host	CaF_2	SrF_2	BaF_2	α-$NaYF_4$	α-$NaYF_4$
Symmetry	O_h	O_h	O_h	O_h(Na)	O_h(Y)
Literature (undoped)	236.6 [33]	251.1 [33]	268.5 [33]	235.7 [34]	235.7 [34]
Calculated (doped)	237.2	240.9	244.0	245.7	231.8

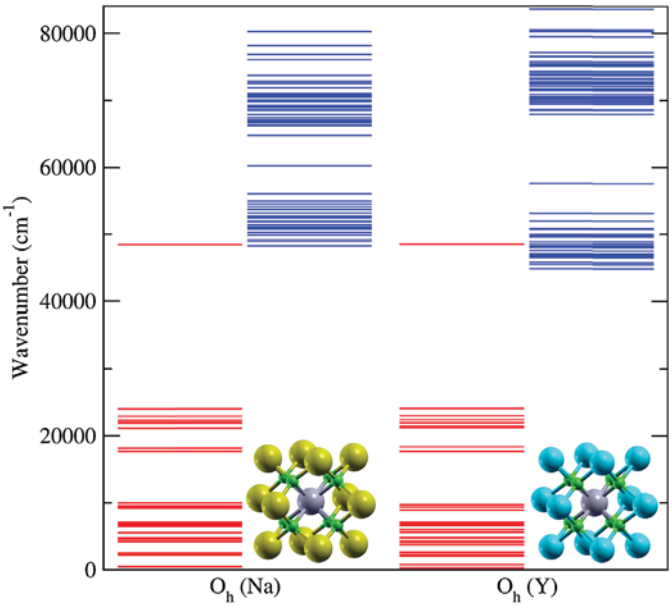

Figure 3. Calculated multiplet energy levels of Pr^{3+} doped α-$NaYF_4$, corresponding to the $[Xe]4f^2$ (red) and the $[Xe]4f^15d^1$ configurations (blue). The two given symmetries differ in the second coordination sphere containing just Na^+ (O_h(Na)) or Y^{3+} (O_h(Y)). The structures represent the central Pr^{3+} ion (grey) surrounded by eight F^- (green) and the second coordination sphere containing Na^+ (yellow) or Y^{3+} (blue). (For interpretation of the references to colour in this figure legend, the reader is referred to the web version of this article.)

still located at about 47 000 cm^{-1} (see Figure 1 and 3). Therefore, the lowest energy level of the $[Xe]4f^15d^1$ configuration is located above the highest energy level $^1S_0$ which means that PCE for this phosphor is present. The emission spectrum of α-$NaYF_4$:Pr^{3+} is dominated by sharp intraconfigurational $[Xe]4f^2$–$[Xe]4f^2$ transitions which is in good agreement with previous results of Sommerdijk et al. [18]. The emission lines in the UV part of the spectral range originate from the $^1S_0$ energy level with the maximum at 24 600 cm^{-1} due to the $^1S_0$–$^1I_6$ transition and representing the first photon. The emission lines in the visible part of the spectral range originate from the $^3P_0$ energy level and representing the second photon. In the UV range at around 43 500 cm^{-1} there is a small amount of broad emission which cannot be assigned to any $[Xe]4f^2$–$[Xe]4f^2$ transition known for Pr^{3+} and which was already described elsewhere [19]. This could lead back to a small amount of interconfigurational $[Xe]4f^15d^1$–$[Xe]4f^2$ emission originating from the lowest energy level of the $[Xe]4f^15d^1$ configuration. In contrary to $LaPO_4$:Pr^{3+} where the combination of sharp intraconfigurational $[Xe]4f^2$–$[Xe]4f^2$ transitions and broad interconfigurational $[Xe]4f^15d^1$–$[Xe]4f^2$ transitions is only observed at low temperatures [38] here this is already occurs at room temperature.

To explain the differences between the above given theoretical results (see Figure 3) and the experimental measurements (see Figure 4), new models were performed assuming a distortion of the O_h symmetry [39]. This distortion originates from the second coordination sphere of Pr^{3+} which consists of 12 sites randomly occupied by Na^+ (132 pm) and Y^{3+} (116 pm). Unlike as mentioned in [40] the second coordination sphere is affecting the anions which are then responsible for the change of the ligand field. Since the ionic radii as well as the ionic charge of these two ions are so different distortion of the symmetry is expected. Taking into account the second coordination sphere, 2^{12} = 4096 different structural conformations are possible, from which only two extreme situations exhibit O_h symmetry. Due to the large number of structural conformations, here we analyze only the situation where the second coordination sphere contains exactly 6 Na^+ and 6 Y^{3+} ions beside the two extreme situations discussed before (for more information see Section 4). The model parameters of the O_h cases (see Table 1) are modified for the distorted conformations using the AOM for the angular distortion and DFT for the radial part. Thus the descent in symmetry goes from D_{3d} to only C_1. The results of these calculations are given in Figure 5.

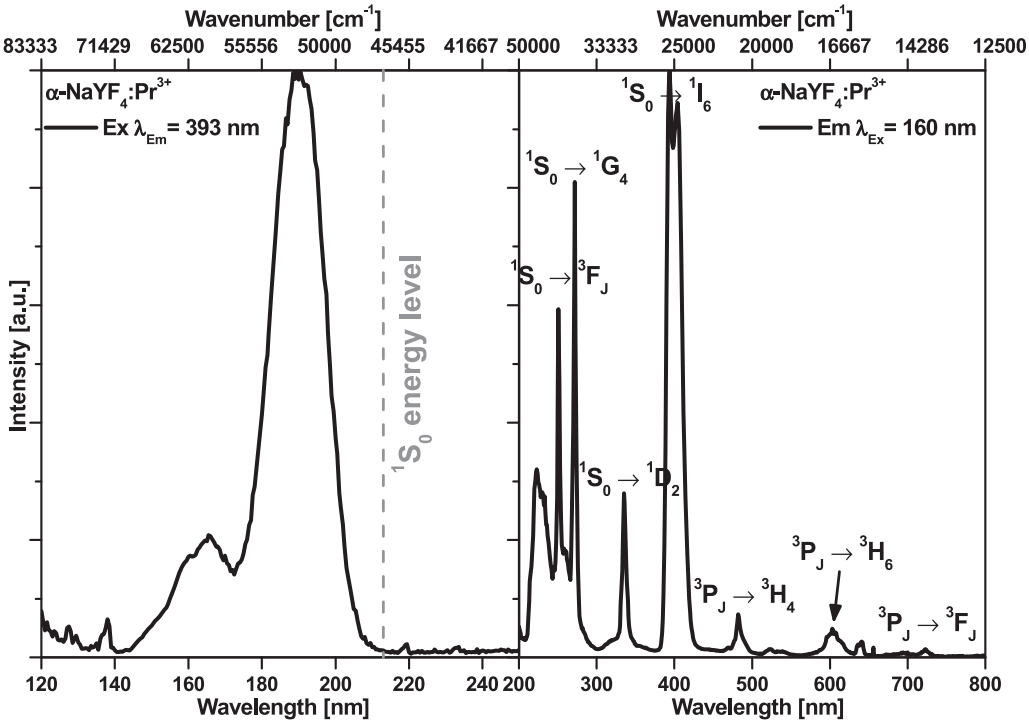

Figure 4. Room temperature luminescence spectra of α-$NaYF_4$:Pr^{3+}(1.0%). VUV excitation spectrum is given on the left and emission spectrum on the right. The dashed grey line represents the energy position of the $^1S_0$ energy level.

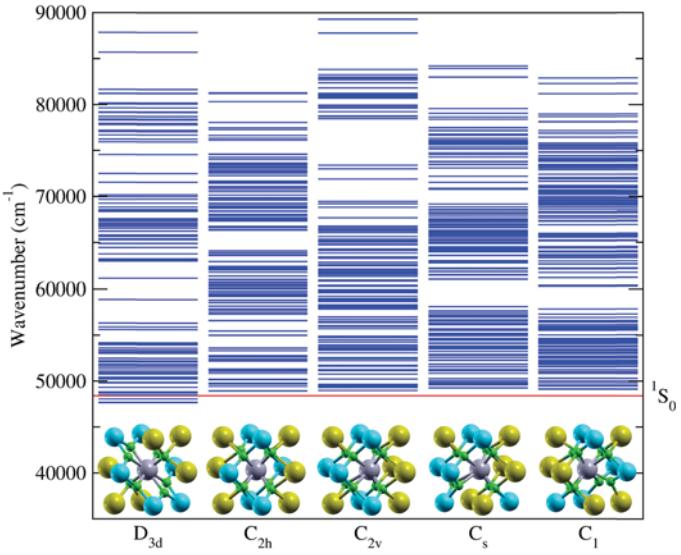

Figure 5. Calculated multiplet energy levels of the $[Xe]4f^1 5d^1$ configurations of the Pr^{3+} doped α-$NaYF_4$ in different symmetries. The solid red line characterizes the energy of the $^1S_0$ energy level of the ground $[Xe]4f^2$ configuration. The structures represent the central Pr^{3+} ion (grey) surrounded by eight F^- (green) and the second coordination sphere containing Na^+ (yellow) and Y^{3+} (blue). (For interpretation of the references to colour in this figure legend, the reader is referred to the web version of this article.)

The multiplet energy levels arising from the $[Xe]4f^2$ configurations is not presented in Figure 5, since the influence of the chemical surrounding is very low. The influence of the chemical surrounding on the 5d orbitals for the given symmetries is much stronger which results for each case in a different splitting. Therefore, we achieve symmetries where the lowest energy level of the $[Xe]4f^1 5d^1$ configuration is located below the highest energy level $^1S_0$ and do not show PCE like D_{3d}. However, for symmetries viz. C_{2h}, C_{2v}, C_s, and C_1 the lowest energy level of the $[Xe]4f^1 5d^1$ configuration is located above the highest energy level $^1S_0$ which leads to PCE (see Figure 5). Notice that lower symmetry structures would also be more common among the 4096 different structural configurations than higher ones. This explains the PCE process in α-$NaYF_4$ as an effect of lowering the symmetry due to the effect of the second coordination sphere, as well as the small amount of interconfigurational $[Xe]4f^1 5d^1$–$[Xe]4f^2$ emission, which would come from Pr^{3+} ions occupying higher symmetry sites.

3. Conclusions

In summary, the alkaline earth fluorides, (CaF_2, SrF_2 and BaF_2) do not show PCE since the Pr^{3+} is located at a crystallographic position with O_h symmetry. The splitting of the 5d orbitals in this symmetry is larger, insofar as the lowest energy level of the $[Xe]4f^1 5d^1$ configuration is always located below the highest energy level $^1S_0$ of the ground $[Xe]4f^2$ configuration. Our calculations fit to the experimental data, which show mainly interconfigurational $[Xe]4f^1 5d^1$–$[Xe]4f^2$ emission. α-$NaYF_4$ offers as well O_h symmetry for the cation position. The calculation of such a system where the Pr^{3+} is located at a crystallographic position with O_h symmetry would lead to a material without showing PCE. This is in contradiction with the experimental data which show mainly intraconfigurational $[Xe]4f^2$–$[Xe]4f^2$ emission lines. By lowering the symmetry starting from a high D_{3d} to the low C_1 this extraordinary finding can be explained. The lower symmetries which describe a distortion of the crystallographic position can be easily explained by the second coordination sphere. Moreover, with these different symmetries it is possible to explain the emission spectra which shows in addition a small part of interconfigurational $[Xe]4f^1 5d^1$–$[Xe]4f^2$ transitions in the UV part of the spectral range.

4. Experimental

4.1. Computational details

VASP calculations were performed to determine the surrounding structure of Pr^{3+} in a periodic lattice. PBE functional was used for the exchange-correlation potential. The Projector Augmented Wave method (PAW) was used to reproduce the interaction of the valence electrons with the nuclei and core electrons. A plane-wave basis set with a cutoff energy of 400 eV was used to reproduce the electronic states. The atomic positions were relaxed until all forces were smaller than 0.001 eV/Å. From the relaxed structure, molecular calculations were performed with ADF 2013.01 to obtain the electrostatic and ligand field parameters. A TZ2P+ basis set was used for Pr, and a TZP basis set was used for F. Point charges are included at the distance of the Pr^{3+} second coordination sphere to reproduce the effect of the lattice potential. The distorted structures of $NaYF_4$ are obtained from molecular calculations by fixing the positions of the Na^+ and Y^{3+} ions in the second sphere, allowing to relax the Pr^{3+} and F^- ions.

4.2. Experimental details

All phosphors were prepared by precipitation from aqueous solution at the Department of Chemical Engineering, Münster University of Applied Sciences. The concentration of Pr^{3+} in the so prepared phosphors was adjusted to 1%.

In case of the alkaline earth fluorides the alkaline earth nitrates, viz. $Ca(NO_3)_2{\cdot}4H_2O$ (ProAnalysi, Merck), $Sr(NO_3)_2$, (ProAnalysi, Merck), and $Ba(NO_3)_2$, (ProAnalysi, Merck), were dissolved in water together with stoichiometric amounts of $Pr(NO_3)_3{\cdot}6H_2O$ (99.9%, Alfa Aesar) and subsequent dropwise addition of dissolved NH_4HF_2 (95%, Alfa Aesar) until precipitation occurred. After filtration and drying 1% NaF was added for charge compensation. The mixtures were then filled into glassy-carbon crucibles and sintered for 6 h at 900 °C in a nitrogen stream. The nitrogen, which was used to avoid the reaction of the fluorides with oxygen, was further purified by drying with molecular sieve and KOH.

For the α-$NaYF_4$ a stoichiometric mixture of $YCl_3{\cdot}6H_2O$ (99.9%, Treibacher Industrie AG) and $PrCl_3{\cdot}6H_2O$ (99.9%, Sigma–Aldrich) was dissolved in water and combined with a solution of a ten times molar excess of NaF (ProAnalysi, Merck). Precipitation occurred immediately and after filtration and drying the mixture was filled into a glassy-carbon crucible and sintered for 6 h at 600 °C in a nitrogen stream. This temperature was chosen to avoid the transformation of the cubic α-phase of $NaYF_4$ to the hexagonal β-phase.

4.3. Characterization

All luminescence measurements were performed at the Department of Chemical Engineering, Münster University of Applied Sciences.

For all luminescence measurements the powder samples were pressed into a PTFE-sample holder, whereby the surface was structured by using a white fleece afterwards. All investigated powder samples were excited at 160 nm and the luminescence spectra recorded with a VUV spectrometer (Edinburgh Instruments FS920). The spectrometer was equipped with a VUV monochromator VM504 from Acton Research Corporation (ARC) and a deuterium lamp as an excitation source. The sample chamber was flushed with dried Nitrogen in order to prevent absorption of VUV radiation by water and oxygen. Excitation and emission spectra were recorded in the ranges of 120–250 nm and 200–800 nm, respectively. The

emission spectra were corrected by using a correction file obtained from a tungsten incandescent lamp certified by NPL. The relative VUV excitation intensities of the samples were corrected by dividing the measured excitation spectra of the samples with the excitation spectrum of sodium salicylate (o-$C_6H_4OHCOONa$) under the same excitation conditions. The measurements were performed at ambient temperature and pressure with a step size of 0.5 nm.

Acknowledgements

This work is supported by the Swiss National Science Foundation (SNF), the Swiss State Secretariat for Innovation and Research, the European Cooperation in Science and Technology (COST) Action EUFEN (CM1006) and the Bundesministerium für Bildung und Forschung (BMBF) project 13N9353. Dr. Fanica Cimpoesu from the University of Bucharest and Dr. Jörg Nordmann form University of Osnabrück are warmly acknowledged for the fruitful discussion and interest on this topic.

References

[1] A. Katelnikovas, H. Bettentrup, D. Dutczak, A. Kareiva, T. Jüstel, J. Lumin. 131 (2011) 2754.
[2] A. Richter, E. Heumann, E. Osiac, G. Huber, W. Seelert, A. Diening, Opt. Lett. 29 (2004) 2638.
[3] T. Sandrock, E. Heumann, G. Huber, B.H.T. Chai, in: P. Payne (Ed.), Adv. Solid State Lasers, Optical Society of America, San Francisco, 1996, PM1.
[4] J.L. Sommerdijk, A. Bril, A.W. de Jager, J. Lumin. 8 (1974) 341.
[5] W.W. Piper, J.A. DeLuca, F.S. Ham, J. Lumin. 8 (1974) 344.
[6] R.T. Wegh, H. Donker, K.D. Oskam, A. Meijerink, Science 283 (1999) 663.
[7] C. Ronda, J. Lumin. 100 (2002) 301.
[8] T. Jüstel, J.-C. Krupa, D.U. Wiechert, J. Lumin. 93 (2001) 179.
[9] B. Herden, A. Meijerink, F.T. Rabouw, M. Haase, T. Jüstel, J. Lumin. 146 (2014) 302.
[10] A.M. Srivastava, W.W. Beers, J. Lumin. 71 (1997) 285.
[11] A.M. Srivastava, D.A. Doughty, W.W. Beers, J. Electrochem. Soc. 143 (1996) 4113.
[12] A.M. Srivastava, D.A. Doughty, W.W. Beers, J. Electrochem. Soc. 144 (1997) L190.
[13] H. Ramanantoanina, W. Urland, A. García-Fuente, F. Cimpoesu, C. Daul, Phys. Chem. Chem. Phys. 16 (2014) 14625.
[14] A.R. West, Grundlagen der Festkörperchemie, Wiley, Weinheim, 1992.
[15] C. Renero-Lecuna, R. Martín-Rodríguez, R. Valiente, J. González, F. Rodríguez, K.W. Krämer, H.U. Güdel, Chem. Mater. 23 (2011) 3442.
[16] A. Grzechnik, P. Bouvier, W.A. Crichton, L. Farina, J. Köhler, Solid State Sci. 4 (2002) 895.
[17] J.K. Lawson, S.A. Payne, Opt. Mater. 2 (1993) 225.
[18] J.L. Sommerdijk, A. Bril, A.W. de Jager, J. Lumin. 9 (1974) 288.
[19] B. Herden, J. Nordmann, R. Komban, M. Haase, T. Jüstel, Opt. Mater. 35 (2013) 2062.
[20] R.D. Shannon, Acta Crystallogr. Sect. A 32 (1976) 751.
[21] P.A. Rodnyi, G.B. Stryganyuk, C.W.E. van Eijk, A.S. Voloshinovskii, Phys. Rev. B 72 (2005) 195112.
[22] S. Schmiechen, P. Pust, P.J. Schmidt, W. Schnick, Nachrichten Aus Chem. 62 (2014) 847.
[23] G. Kresse, J. Hafner, Phys. Rev. B 47 (1993) 558.
[24] G. Kresse, J. Furthmüller, Phys. Rev. B 54 (1996) 11169.
[25] J.P. Perdew, K. Burke, M. Ernzerhof, Phys. Rev. Lett. 77 (1996) 3865.
[26] C.F. Guerra, J.G. Snijders, G. te Velde, E.J. Baerends, Theor. Chem. Acc. 99 (1998) 391.
[27] G. te Velde, F.M. Bickelhaupt, E.J. Baerends, C. Fonseca Guerra, S.J.A. van Gisbergen, J.G. Snijders, T. Ziegler, J. Comput. Chem. 22 (2001) 931.
[28] H. Ramanantoanina, W. Urland, F. Cimpoesu, C. Daul, Phys. Chem. Chem. Phys. 15 (2013) 13902.
[29] H. Ramanantoanina, W. Urland, A. García-Fuente, F. Cimpoesu, C. Daul, Chem. Phys. Lett. 588 (2013) 260.
[30] S. Hüfner, Optical Spectra of Transparent Rare Earth Compounds, Elsevier, New York, 2012.
[31] R.D. Cowan, The Theory of Atomic Structure and Spectra, University of California Press, Berkeley, 1981.
[32] H. Ramanantoanina, W. Urland, F. Cimpoesu, C. Daul, Phys. Chem. Chem. Phys. 16 (2014) 12282.
[33] B.P. Sobolev, E.G. Ippolitov, B.M. Zhigarnovskii, L.S. Garashina, Izv. Akad. Nauk. SSSR Neorg. Mater. 1 (1965) 362.
[34] R.E. Thoma, G.M. Hebert, H. Insley, C.F. Weaver, Inorg. Chem. 2 (1963) 1005.
[35] K.D. Oskam, A.J. Houtepen, A. Meijerink, J. Lumin. 97 (2002) 107.
[36] E. Loh, Phys. Rev. 158 (1967) 273.
[37] S. Kück, I. Sokólska, Appl. Phys. A 77 (2003) 469.
[38] A.M. Srivastava, A.A. Setlur, H.A. Comanzo, W.W. Beers, U. Happek, P. Schmidt, Opt. Mater. 33 (2011) 292.
[39] G.F. Koster, J.O. Dimmock, R.G. Wheeler, H. Statz, The Properties of the Thirty-Two Point Groups, MIT Press, Cambridge, MA, 1963.
[40] D. Tu, Y. Liu, H. Zhu, R. Li, L. Liu, X. Chen, Angew. Chem. 125 (2013) 1166.